Fusion Engineering and Design 200 (2024) 114190

Contents lists available at ScienceDirect

Fusion Engineering and Design

journal homepage: www.elsevier.com/locate/fusengdes

Deterministic analysis of residual heat removal from activated EU DEMO WCLL BB segments during ex-vessel LOCA

Martin Draksler [a,*], Boštjan Končar [a], Christian Bachmann [b], Ivo Moscato [b], Sergio Ciattaglia [b], Alex Valentine [c]

[a] Reactor Engineering Division, Jožef Stefan Institute, Jamova cesta 39, SI-1000, Ljubljana, Slovenia
[b] Eurofusion – Programme Management Unit, Boltzmannstrasse 2, 85748 Garching, Germany
[c] UK Atomic Energy Authority, Culham Science Centre, Abingdon OX14 3DB, UK

ARTICLE INFO

Keywords:
DEMO
LOCA
Residual heat removal
Breeding blanket
BB

ABSTRACT

The residual heat removal from the activated EU DEMO WCLL breeding blankets (BB) in the event of impaired cooling due to an ex-vessel Loss of Coolant Accident (LOCA) is investigated. The postulated guillotine break of a large coolant pipe of the BB Primary Heat Transfer System (PHTS) outside the vacuum vessel (VV) leads to an immediate loss of cooling in one (out of two independent) BB cooling loops. Consequently, every second BB segment (in the toroidal direction) is assumed to be affected. To mitigate the consequences, the plasma rampdown is initiated and the VV is filled with helium to enable the natural convection cooling of the passive BB segments by the circulating gas. A transient conjugate heat transfer analysis with the ANSYS Fluent code has been conducted to assess the thermal response of the affected BB segments and to quantify the effectiveness of the natural convection cooling in respect to thermal radiation and heat conduction through supports. The feasibility of the proposed helium cooling solution for the residual heat removal from the activated BB segments is investigated and a comparison with a conservative study where all BB segments are assumed to be affected by LOCA is discussed.

1. Introduction

The European Demonstration Fusion Power Plant (DEMO) is acknowledged as a crucial milestone in the progression from ITER toward the utilization of fusion energy for safe and efficient production of electricity [1], aiming to provide a demonstration of functionality of all relevant supporting technologies over the plant lifetime [2]. The pre-conceptual DEMO design has been proposed considering (among others) the requirements for rapid and reliable maintenance using manipulators [3,4], long pulse operation and self-sufficient tritium production [5]. Extremely high neutron irradiation of in-vessel components (IVCs) during the operation that is needed to achieve the required tritium breeding ratio in breeding blanket (BB) [6] will result in substantial material activation and high decay heat generation. As such, the BB maintenance is planned to take place several weeks after plasma shutdown [7], when the decay heat is decreased substantially due to absence of short-lived isotopes.

Safety considerations for nuclear fusion reactors shall address among others also the residual heat removal from in-vessel components immediately after plasma shutdown [8]. The safety studies performed to assess the safety and environmental impact of DEMO design options address an exhaustive set of reference accident sequences [9], including the ones considering the malfunction of Primary Heat Transfer Systems (PHTS) of the breeding blanket, divertor (DIV) and vacuum vessel (VV). Among the 21 events reported in [9], two of them (i.e. LB01 and LB03) address an ex-vessel loss of cooling accident from the BB PHTS, resulting in a somewhat reduced heat removal from the activated breeding blanket.

The use of three-dimensional (3D) computational fluid-dynamics (CFD) tools for studying the evolution and consequences of accidents in fusion reactors (including LOCA) is generally avoided due to the high computational requirements. Instead, integral system-level computational tools such as the MELCOR code [10] for severe accidents are preferred. There are many examples of safety studies using the system-level codes. The MELCOR code was used to analyze the consequences of an in-box LOCA for the Water-Cooled Lead–Lithium (WCLL)

* Corresponding author.
E-mail address: martin.draksler@ijs.si (M. Draksler).

https://doi.org/10.1016/j.fusengdes.2024.114190
Received 25 September 2023; Received in revised form 19 December 2023; Accepted 19 January 2024
Available online 25 January 2024

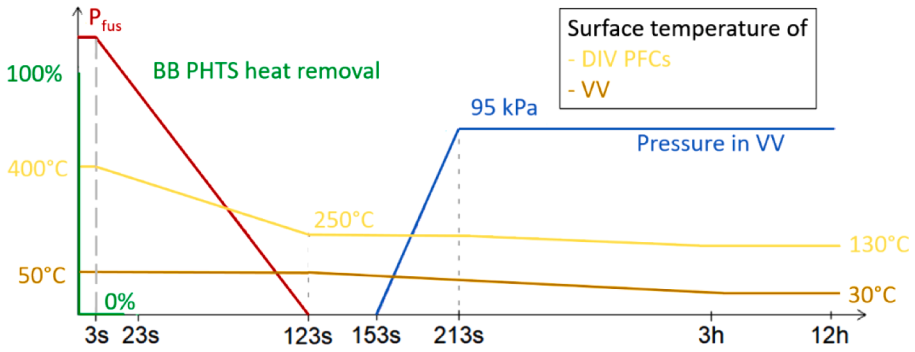

Fig. 1. Overview of the considered LOCA scenario.

blanket concept of the EU DEMO reactor [11]. D'Onorio et al. [12] developed a thermal-hydraulic model of the EU-DEMO tokamak building to investigate pressurization of the tokamak building and radiological releases during the loss-of-coolant accident in EU DEMO WCLL reactor design. The BB LOCA was investigated as a design basis accident for the reference design of the EU DEMO Helium-Cooled Pebble Bed (HCPB) blanket [13]. The system code MELCOR was also used in another study [14], which addressed the evolution of the ex-vessel LOCA for the European DEMO HCPB Blanket Concept, where a double-ended guillotine break of the main pipe in an outboard (OB) loop of the PHTS leads to helium blowdown into the tokamak cooling room and a fast plasma shutdown. Though widely used, system-level codes rely on a number of empirical correlations and simplifications that are not always validated for fusion related applications. In this respect, fully 3D CFD simulations can provide far more accurate and reliable results as they are based on the underlying mechanisms of fluid mechanics. To the best of our knowledge, the only existing CFD study of a LOCA event for EU DEMO reactor is reported in [15], where the inflow of helium due to the in-vessel failure of the first wall (FW) of the EU DEMO HCPB breeding blanket is studied. The authors developed a simplified transient CFD model for the purpose of validating a system-level code, which has been extensively used to study the consequences of the accident.

The current study presents the first CFD analysis of the so-called ex-vessel LOCA scenario, considering an instantaneous loss of cooling from the activated BB segments during plasma operation. The postulated guillotine break of a large BB PHTS coolant pipe outside the vacuum vessel causes an immediate loss of cooling in one (out of the two independent) BB cooling loops. Consequently, it is assumed that only every second BB segment (in toroidal direction) is affected by LOCA, while the other IVCs remain actively cooled. Due to decay heat resulting from material activation, the affected BB segments are internally heated. After LOCA detection, a soft plasma shutdown is automatically initiated. For mitigation of consequences (i.e. to limit the peak BB temperatures and potential damage), the vacuum vessel is filled with helium once the plasma ramp-down is completed, allowing the (affected) BB segments to be cooled by natural convection of circulating gas. It is assumed that the pressure in the VV at the end of the so-called injection phase is equal to 95 kPa [16]. It should be also acknowledged that the VV Pressure Suppression System (VVPSS) design for DEMO is currently under reconsideration. Previously defined intervention setpoint of the VVPSS bleed lines had been set to 90 kPa [17], while in ITER, for example, the present operating limit for the intervention of the bleed lines is set to 0.5 bar

The main objective of this study is to investigate the effectiveness of the proposed mitigation strategy, using a filled gas for removing residual heat from the activated breeding blanket during the ex-VV LOCA occurrence in DEMO. Based on transient CFD analysis, the time-dependent temperature distributions in the affected BB segments and redistribution of heat loads have been assessed. The results of the analysis are compared with the conservative scenario [18–20], where it has been assumed that all BB segments (not every second one) would lose their cooling due to the LOCA occurrence that corresponds to the DEMO design where the BB PHTS would have only one main feed line.

The transient conjugate heat transfer analysis of natural convection cooling inside the vacuum chamber is performed with the ANSYS Fluent code 2021.R2 [21]. To account for the radiation exchange in the closed vacuum vessel the Surface-to-Surface (S2S) radiation heat transfer model [19] has been used. To accurately model the decay heat distribution in the different BB layers, adopted from nuclear analysis [20], the segmentation of the individual BB segments in the poloidal and radial directions was considered. Therefore, one tokamak sector with 5 physical BB segments is further divided into 264 BB sub-segments. Based on consideration of the Water-Cooled Lithium-Lead (WCLL) breeding blanket concept [22], the homogenized material properties are applied. Developed model considers the refined ("realistic") decay heat data [23] and temperatures of IVCs [16]. It is also assumed that BB PHTS comprises two independent cooling loops, each of them connected only every second BB segment in toroidal direction.

Section 2 of this article provides a detailed description of considered scenario. In Section 3 the CFD simulation model is described. Results of analysis are presented in Section 4 and the conclusions are given in Section 5.

2. Description of scenario

The ex-VV LOCA event is initiated by a guillotine break of a large coolant pipe of the Primary Heat Transfer System (PHTS) outside the vacuum vessel [16,24]. When the leak in PHTS occurs, the coolant pressure decreases due to the coolant discharge. A leak in the PHTS BB is detected by pressure sensors in the coolant when the coolant pressure in the PHTS drops below 130 bar At this point, a soft plasma ramp-down is automatically initiated. When the PHTS coolant pressure is further reduced to the coolant saturation pressure (~110 bar), the isolation valves on the external walls of the tokamak building isolate all secondary cooling loops, the main PHTS pumps are switched off (within ~20 s) and the shutdown cooling system is used to cool the reactor. In case of a large guillotine break, both detection points (at about 130 and 110 bar) are reached after 1–2 s and cannot be distinguished. Once the coolant pressure is reduced to 110 bar, the coolant changes its state from liquid to vapor. Release of steam through the leak progressively reduces the vapor pressure inside the PHTS until all coolant capacity is lost. In the present study, it is conservatively assumed that the drop of the heat removal capacity is instant, and occurs at exactly at the same time as the LOCA.

The course of the LOCA scenario considered is shown in Fig. 1. The red curve shows the gradual plasma shutdown, which is triggered 3 s after the detection of LOCA and is assumed to last 120 s. Other in-vessel components maintain nominal cooling capability until the plasma ramp-down is completed. The VV PHTS is assumed to remain operational and capable to remove the decay heat from the tokamak. After the plasma

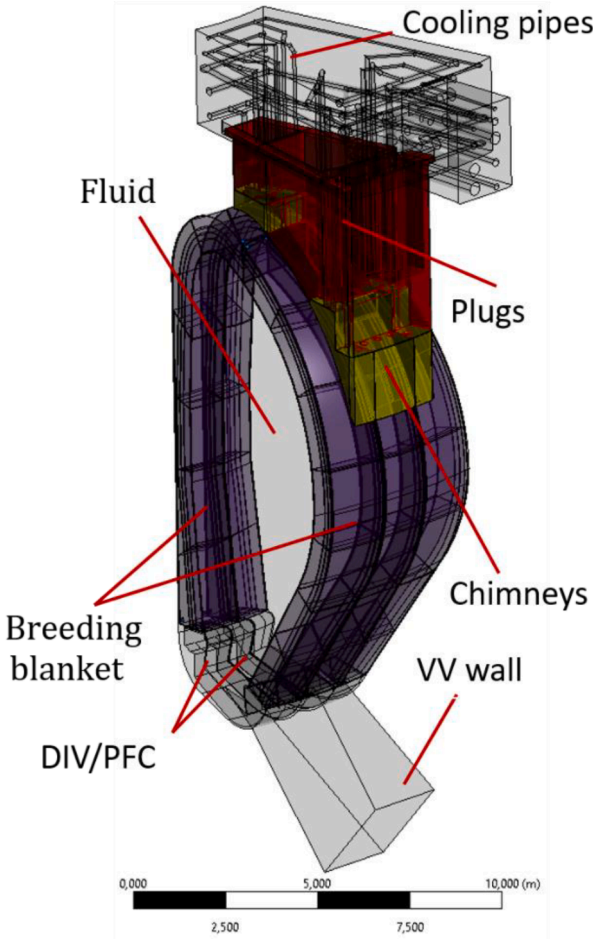

Fig. 2. Computational domain with main in-vessel components.

shutdown is completed the VV temperature (brown curve) will be reduced by 5 °C per hour until it finally reaches 30 °C. The foreseen time evolution of DIV PFC surface temperature is shown with yellow line.

Helium at ~200 bars is stored at 50 °C in dedicated storage tanks with a total volume of about 30m^3, sufficient to fill the VV at a pressure of 95 kPa. The tanks are located in the tokamak building and are connected by pipes to upper ports. Double valves in the pipes are opened 30 s after the completion of the plasma ramp-down (at 153 s) to fill the VV with helium at 95 kPa within 60 s. The expected (assumed) pressure evolution in the VV is shown by the blue curve in Fig. 1. Once the helium injection is completed (closed valves), the natural convection inside the VV is established, transferring heat from passive (internally heated) in-vessel components to the actively cooled VV. Heat removal from the reactor is eventually achieved by safety-classified VV PHTS [25].

3. Simulation model

In the conducted LOCA analysis, the injection of helium into plasma chamber is not explicitly considered. Instead, it is conservatively assumed that the VV remains evacuated till the completion of the so-called helium injection phase. During the initial 213 s of accident, the cooling of affected BB segments by LOCA is exclusively accomplished through thermal radiation. At the end of the injection phase, the domain is instantaneously filled with helium at a pressure 95 kPa. The helium temperature is set to 200 °C and pressure to 95 kPa, both representing the re-initialization of helium conditions for the follow-up phase of the simulation run. Helium temperature has been estimated from additional analyses (CFD and analytical) where only the helium injection phase has been analysed [26].

In this study [26], the helium with temperature 50 °C is being injected into initially evacuated VV. The injection phase ends when the pressure in VV is 95 kPa. Aiming at a reduction of the computational cost, only the most inner part of the VV is considered as a free volume for helium injection (i.e. the gaps between adjacent BB segments, individual BB segments and the VV walls were neglected). As such, the external walls of the simulation domain are represented by the front wall surfaces (FW) of the breeding blankets and the external surfaces of the divertor cassettes (PFC), which both contributed to helium heat up. This simplified study [26] has shown that the volume average temperature of the helium in VV (once the pressure reached 95 kPa) is 200 °C. Since the pressure in helium tanks is very high while the VV is initially evacuated, the flow at the nozzle throat is choked. Thus, an analytical model for the ideal, adiabatic nozzle was used to calculate the occurring (theoretical) mass flow rate at the nozzle throat in respect to the pressure build-up in the VV and due to its decrease in the storage tank.

To simulate the transonic helium injection into VV that is expected to occur in the considered case, a temporal and spatial discretization of a very high resolution is needed. Especially challenging is a very small time-step of the simulation (~1 μs) required to adequately resolve the induced pressure shocks. Otherwise, the simulations diverge or predict wrong realization of the injected flow. Such simulations require considerably smaller time step, far too small to simulate transients of several hours in physical time, as is needed for the LOCA analysis.

It should be also noted that the vacuum conditions cannot be simulated with the conventional CFD models due to the limitation of the Knudsen Number (i.e. the model is valid only for conditions following the so-called Continuum Flow Model). In the present LOCA study, the vacuum condition in VV (maintained during the initial 213 s of transient) is modelled by setting the thermal conductivity of fluid close to zero (e.g. to 10^{-12} W/mK).

3.1. Geometry and applied boundary conditions

This study utilizes the DEMO baseline 2017 geometry with 16 equatorial sectors. The geometry model, shown in Fig. 2, considers one equatorial sector of the DEMO tokamak that is closed at the level of the upper port ring channel. Each sector includes five BB segments, i.e. 3 BB segments in the outboard blanket (OB) and 2 segments in the inboard blanket (IB). To reduce the computational cost of simulations, the in-vessel components that are kept at constant temperature (i.e. actively cooled BB segments and divertor cassettes with Plasma Facing Components) are supressed from the model. Instead, the corresponding fluid wall boundaries are modelled as the no-slip walls with prescribed temperature. In the same manner, the no-slip walls with prescribed temperature are applied at the inner walls of the VV, whereas the outer surfaces of the cooling pipes located within the upper port are represented as adiabatic no-slip walls. Other in-vessel structures (i.e. upper port plugs, segment chimneys and supports) are treated as passive elements that engage in heat exchange with the circulating fluid and neighbouring components. Symmetry boundary condition is applied to both lateral boundaries of the fluid domain.

For a better consideration of the decay heat data, the segmentation of each BB segment in radial and poloidal directions is applied as possible similar to that used in the nuclear analysis [23].

3.2. Homogenized material properties

The material composition of the individual blanket components is adopted from the nuclear analysis [23]. The water is removed from all components and the thermophysical properties are adjusted accordingly [18]. The homogenized properties are computed using the methodology presented in [7]. Void spaces formed by drained fluids are treated as empty regions, characterized by having zero thermal conductivity, specific heat, and density. The volumetric compositions for each component of the breeding blanket together with the homogenized

Table 1
Material composition and applied homogenized properties of each of the breeding blanket components.

		vol% composition				Homogenized properties		
	Component	Tungsten	LiPb	H20	Eurofer	ρ [kg /m^3]	C_p [J /(kg K)]	λ [W /(m K)]
IB/OB	**FWA**	100	0	0	0	19,290.0	139.0	149.0
IB	**FW/side walls**	0	0	6.77	93.23	7164.7	574.0	23.5
	Breeder zone	0	86.90	1.18	11.92	9465.3	227.0	16.1
	PbLi manifold	0	80.06	1.21	18.73	9315.7	249.1	16.8
	H2O manifold	0	0	64.14	35.86	2755.8	574.0	9.0
	BSS	0	0	5.54	94.46	7259.3	574.0	23.8
OB	**FW/side walls**	0	0	6.09	93.91	7217.0	574.0	23.7
	Breeder zone	0	87.63	1.41	10.96	9463.3	224.0	15.9
	PbLi manifold	0	79.69	1.13	19.18	9313.9	250.6	16.8
	H2O manifold	0	0	64.31	35.69	2742.8	574.0	9.0
	Breeder zone	0	0	4.97	95.03	7303.1	574.0	23.9
	Supports	SS316				8000.0	500.0	20.0
	Plugs	Al				2719.0	871.0	202.4
	Chimneys	SS316				8000.0	500.0	16.3

Table 2
Overview of mesh parameters.

	No. of elements	Min orth. quality	Surface element size	Element size in Fluid [m]	Element size in BB [m]	No. of elements in fluid gaps
Mesh1	4057,861	0.15	0.02–0.58	-	–	2
Mesh2	3627,745	0.12	0.02–0.58	0.05–0.5	–	2
Mesh3	42,983,792	0.15	0.01–0.5	0.01–0.5	0.01–0.5	7
Mesh4*	40,217,465	0.15	0.01–0.5	0.01–0.5	0.01–0.5	7

* Mesh includes “hex-core”.

Table 3
Mesh study – predicted fluid/BB temperatures.

	T_{avg} [°C] @ Fluid	T [°C] @ BB
Mesh1	956	265–2678
Mesh2	987	267–2704
Mesh3	964	259–2666
Mesh4	965	261–2670

properties are reported in Table 1.

The fluid is treated as compressible (modelled as an ideal gas), so the fluid density depends on the local pressure and temperature [21]. The helium is considered to have temperature-dependent viscosity [26] and thermal conductivity [27]. However, no significant difference in predicted peak temperatures of BB segments were observed when constant thermophysical properties for helium were used [18].

3.3. Numerical mesh

Fully conformal meshes have been generated with the “Fluent with meshing” software [14], by using the “Watertight workflow”. The mesh characteristics are specified by the surface mesh parameters, mesh refinements are applied locally with the so-called “proximity” option, and additionally with boundary layers. All generated meshes are built of polyhedral cells, and the hex-core option has also been tested. Eventually, at least three cells are applied across the thickness of individual BB sublayer, and up to seven cells are used across (2 cm wide) gaps in the fluid domain (e.g. in channels between adjacent BB segments, BB back walls and the VV wall). In the case of refined meshes (i.e. Mesh3 and Mesh4), three prism layers are placed at the fluid side of all fluid/solid interfaces. Totally, four different meshes have been tested in the frame of steady-state numerical analysis. Characteristics of the tested meshes are presented in Table 2.

In the mesh sensitivity study, the internal heat generation is only

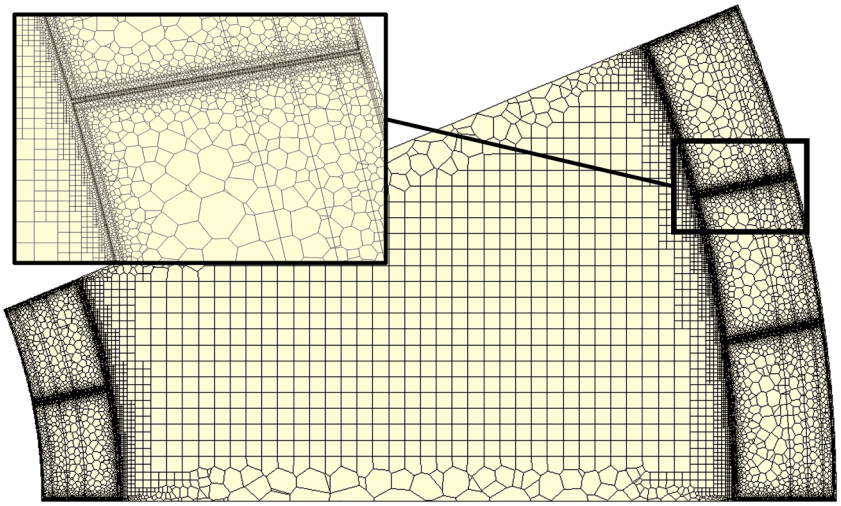

Fig. 3. Horizontal slice through the mesh used in the transient analysis.

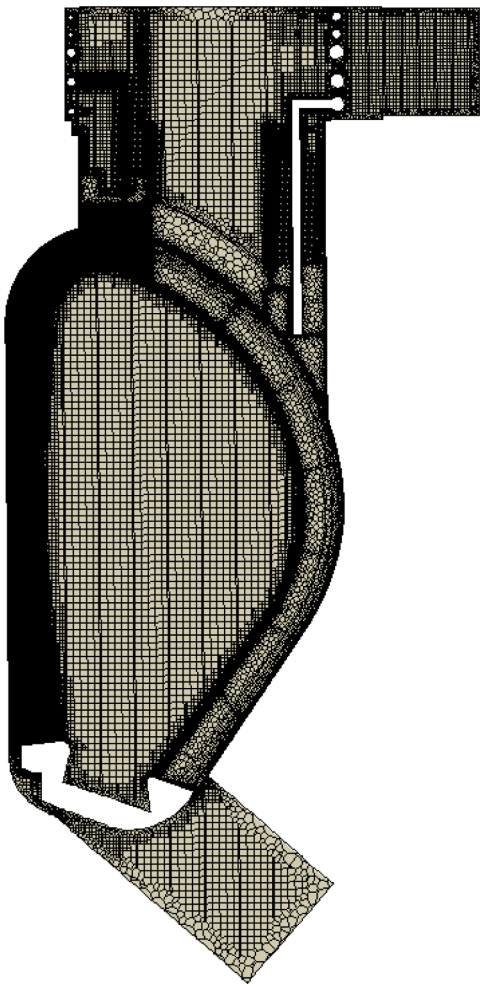

Fig. 4. Vertical slice through the mesh used in the transient analysis.

applied to specific BB sublayers to reduce the obtained peak BB temperatures. In our simulations the time-dependent decay heats from neutronic computations are used, which were scripted in external files and imported to the Fluent code. The steady-state simulation considers only the scripted value at time 0 s, which corresponds to the volumetric heat generation rates immediately after the plasma shutdown. In a steady-state simulation such values (which do not decrease in time) resulted in non-realistically high temperatures of BB segments. Therefore, for the purpose of the mesh sensitivity study the decay heat is applied only to certain BB sublayers. Alternatively, lower heat generation rates, corresponding to later times after the plasma shutdown, could be used.

As presented in Table 3, the lowest peak BB temperatures are obtained with both high-resolution meshes, which have 7 elements across the fluid gaps. It has also been shown (Mesh1 vs. Mesh2) that larger elements in the fluid domain (if minimum size increased from 0.02 m to 0.05 m) yield to ~25 °C higher predicted peak BB temperature. The obtained results are in agreement with our previously conducted 2D steady-state mesh sensitivity study of a laminar flow in a 5 m long and 2 cm wide channel [7] and with the study reported in [28], where it has been shown that somewhat coarser fluid mesh leads to under-predicted heat transfer rates at the fluid-solid interface and higher temperatures of passive solid structures. Both high resolution meshes (Mesh3 and Mesh4) are generated with identical settings, except that hex-core is applied in the latter case, which has a positive effect on the convergence of the solver. Therefore, the Mesh4 is used in transient analysis.

Snapshots of the Mesh4, which is used in transient analysis, are shown in Figs. 3 and 4.

Table 4
Initial conditions - Components' average temperatures prior to the ex-VV LOCA.

Layer/Component	Initial temperature [°C]
FWA, FW	380
Side plates	300
Breeder zone, LiPb manifolds	450
H_2O manifolds, BSS	300
Divertor PFCs/Cassette body	400/200
VV	50

3.4. CFD model settings

Transient analysis of the natural convection cooling of passive BB segments together with the radiation heat transfer has been performed with the ANSYS Fluent code 2021.R2 [21]. Since the estimated global Rayleigh number ($\sim 6 \times 10^5$) in the domain is below the threshold (10^9) determining the transition between the laminar and turbulent natural convection in a closed cavity [21,29], the flow in the present study is considered laminar.

Conjugate heat transfer simulations were conducted employing the PISO algorithm in combination with a fixed time-stepping approach and PRESTO! pressure scheme [21]. Time integration of governing equations is obtained with the second order implicit scheme. The so-called frozen-flux formulation and "Warped-Face Gradient Correction" are used for better stability. Advanced solver settings include also the neighbor and skewness correction set to unity with enabled "Skewness-Neighbor Coupling". The residual convergence criterium for continuum and momentum equations is set to 10^{-5}, for energy equation the target value is one order of magnitude smaller.

In the initial 213 s of simulation (see Fig. 1), the vacuum conditions in the vacuum vessel are modelled by setting the thermal conductivity of the helium close to zero, so that only the radiation heat transfer between the solid surfaces inside the VV is resolved using a fixed time step of 0.5 s. In the following sequence of the simulated transient, the natural convection of circulating helium in the VV is resolved together with the radiation heat transfer. In order to prevent solver divergence once the helium motion is being resolved and the natural convection is not yet well established, very small simulation time step is needed. During the first second of transient phase with helium inside the plasma chamber the simulation time step has been successively increased from the initial 10^{-8} s to 10^{-4} s.

For faster progression in physical time during the simulation, the so-called frozen-flow treatment has been used [7]. The main idea behind this time stepping approach is that the flow field is temporarily frozen for certain number of time steps, when only the heat transfer equations are being solved considering previously obtained flow field and thus the simulation time step can be "substantially" increased. After that, the full set of conservation equations (Navier-Stokes equation and heat transfer equations) is solved again, which requires increased time resolution. In this study, the flow freezing is applied repeatedly every 100 time steps, of which 75 time steps are performed with the simulation time step increased from 10^{-4} s to 0.5 s, followed by 25 time steps when fluid motion is resolved. More details about the approach used are available in [7,20]. This strategy has been tested in our previous study [20], where the effect of the flow freezing has been verified against the solution obtained without the frozen-flow assumption. It has been shown that the difference in predicted maximum BB temperature between both cases, reported one hour after the beginning of transient, is less than 1 °C. While investigating the effect of flow-freezing period [20], it has been shown that with the increase of flow freezing period by a factor of 10 (while keeping the flow resolving period unchanged) approximately 10 °C different peak temperature is obtained after 3.84 h of simulated time.

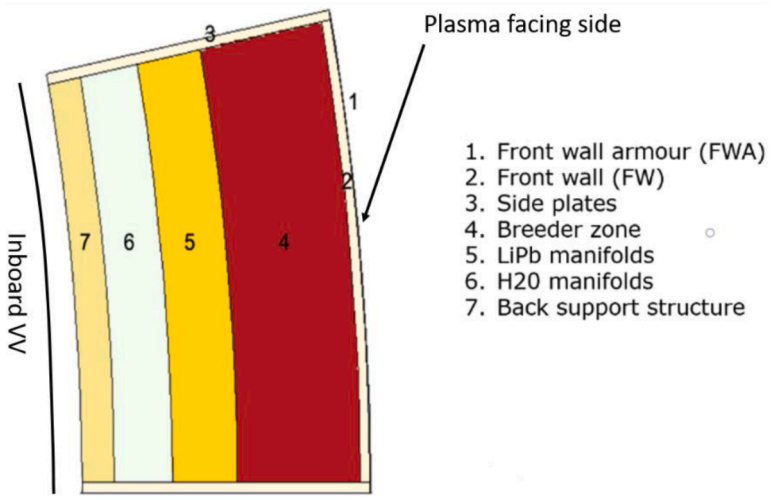

Fig. 5. Homogenized WCLL blanket layers as implemented in the MCNP model and Fluent simulation. Adapted from [23].

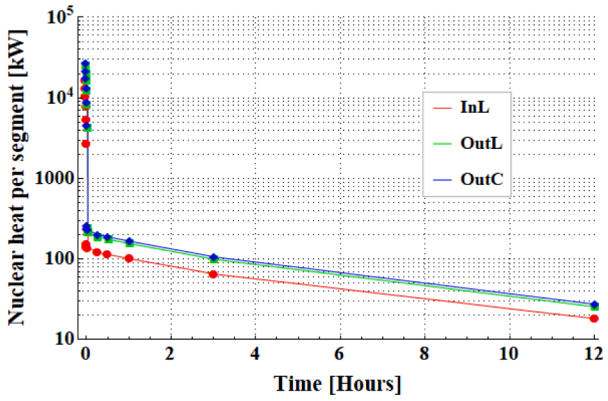

Fig. 6. Total heating per unit of time in individual WCLL BB segments after plasma shutdown.

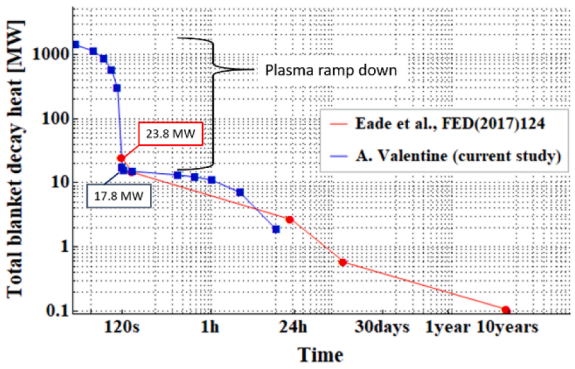

Fig. 7. Comparison of nuclear heat data from literature. Sources: Eade et al. [31], A. Valentine [23].

To account for the radiation exchange in the closed vacuum vessel the Surface-to-Surface (S2S) radiation heat transfer model [21] has been used. It is assumed that all emitters (i.e. the steel or tungsten walls of the VV, divertor and blanket) are gray-diffuse surfaces with emissivity set to 0.3 [24]. Up to 10 energy iterations are performed per radiation iteration, with maximum number of radiation iterations set to 15. To reach the target residual convergence criteria for the S2S model set to 10^{-3}, in average up to 14 iterations were needed. The initial temperatures of the components [24] are provided in Table 4.

3.5. Thermal loads in BB segments (decay heat data)

The heating of the breeding blanket has two contributions: the nuclear heating from neutrons and photons and the decay heat resulting from material activation. The former is only present in operations while the decay heat persists after shutdown. These are calculated through nuclear analysis [19] using the Monte Carlo N-Particle® (MCNP) model [30] for the DEMO WCLL reference model with homogenised blanket layers. The referenced study [23] has been performed specifically for the assessment of the nuclear heating and decay heat in the WCLL DEMO blanket modules in the event of an ex-vessel LOCA, when all water is assumed to be removed from the blanket. For better consideration of the nuclear heat data in the CFD study, the heating densities are reported for individual blanket layers at a poloidal resolution of 1 to 2 m, which means that six or seven poloidal subsegments were introduced for the inboard and outboard modules, respectively.

Homogenised WCLL blanket layers are illustrated in Fig. 5, showing a horizontal slice through the inboard BB segment. The outboard segmentation differs only in radial thickness of the layers and material. Material composition of each of the blanket components is presented in Table 1. The CFD model does not explicitly incorporate the 0.5 mm thick front wall armor (FWA). Therefore, additional volumetric energy source, representing the generated decay heat in FWA, is specified at the front wall-fluid interface [19].

The time course of applied nuclear heating in the individual BB segments is presented in Fig. 6. The two-minute plasma ramp-down allows the short-lived isotopes to decay, resulting in a lower decay heat immediately after shutdown [23] relative to instantaneous shutdown as generally assumed for nuclear analysis. This can be clearly observed in Fig. 7, where the applied nuclear heat data [23] are compared with the results of a previous nuclear analysis [31] for the WCLL BB design where the plasma is turned off at a certain point in time. It should be noted that in the study by Valentine [23], it is assumed that the water is drained from the BB segments, while in the study by Eade [31], the undrained BB segments were considered.

4. Results

4.1. Considered scenarios

The simulation model includes only one equatorial sector of the DEMO tokamak with 5 BB segments. Thus, two simulations have been performed to consider both possible geometrical combinations of BB

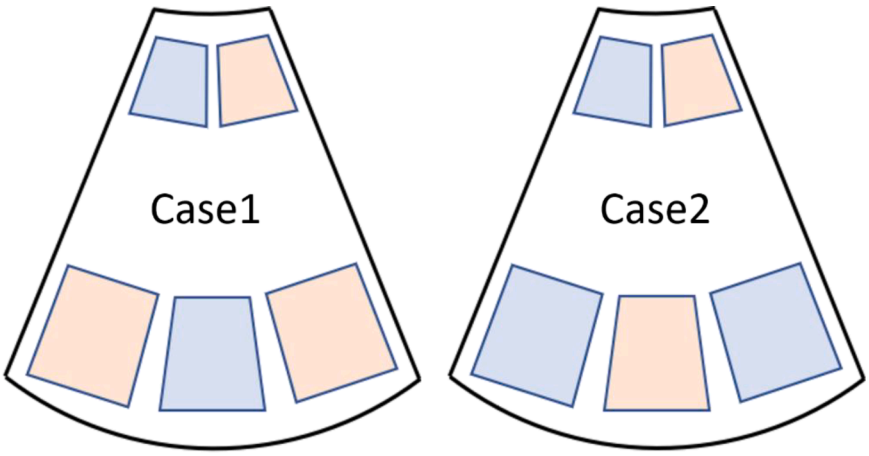

Fig. 8. Considered scenarios in the analysis, showing different combinations of BB segments that are affected by the ex-VV LOCA. Actively cooled BB segments are shown with blue color.

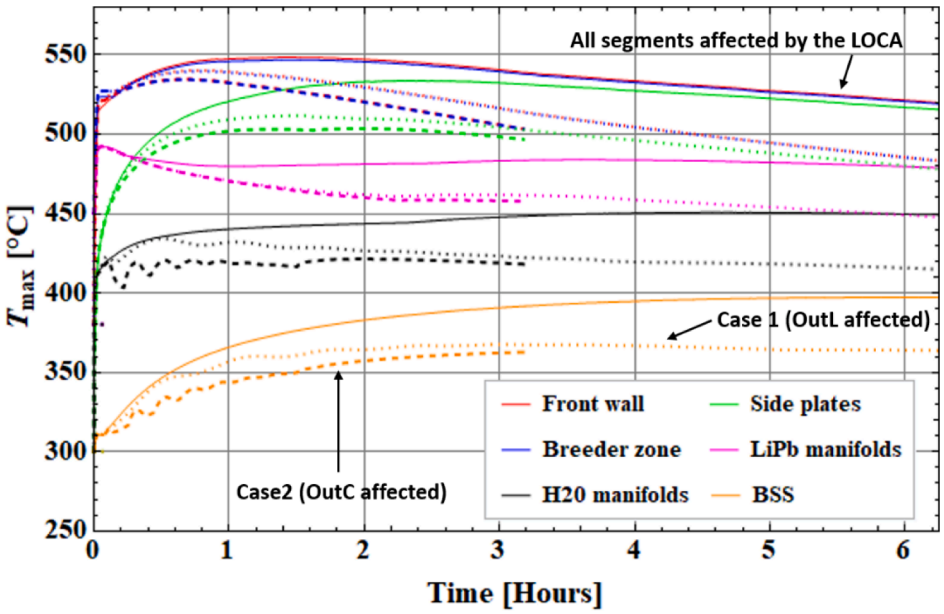

Fig. 9. Time history of peak temperatures in individual blanket layers for inboard segment (InR). Solid lines indicate the solution of the conservative case where all segments are assumed to be affected by the LOCA. Dotted lines indicate the analysis for the Case1, where BB PHTS leakage affected one inboard (InR) and both lateral outboard segments (OutL/OutR). Dashed lines indicate the results of the analysis for the Case2, where the central outboard (OutC) segment is affected by the LOCA in addition to the InR segment.

segments affected by the ex-VV LOCA (see Fig. 8). For both considered cases, it is assumed that one of the inboard BB segment (InR) is affected by the LOCA, while the other remains (InL) actively cooled. For the outboard BB segments, in the first considered case (i.e. Case1), it is assumed that both outboard lateral (OutL/OutR) segments are affected by the LOCA, while for the Case2 the cooling of the central outboard (OutC) segment is impaired due to the LOCA occurrence.

4.2. Time trends of peak BB temperatures

CFD simulations have been performed for up to six hours of physical, which has been found to be a sufficiently long period to demonstrate that the occurring natural convection and thermal radiation provide sufficient heat removal to allow the BB segments (affected by the decay heat) to eventually start to cool down.

Time trends of the obtained peak temperatures in the individual blanket layers for the inboard (InR), outboard lateral (OutL) and central outboard (OutC) segments are shown in Figs. 9–11, respectively. For comparison, the results of a conservative analysis [18,19] are presented, where all BB segment are assumed to be affected by the LOCA occurrence.

For all considered cases, the highest temperature in the BB segment is reached within the first two hours of the LOCA accident. Locally, the segment is the hottest near the interface between the Breeder zone and the Front wall, where the peak temperature reaches ~555 °C. This can be seen in Figs. 9, 10 and 11, where the blue (Breeder zone) and red lines (Front wall) overlap. In general, obtained peak BB temperatures for the conservative case are approximately 20 °C higher than in the cases (Case1 and Case2) where only every second BB segment is affected by LOCA.

The oscillations with a time period in the order of ten minutes, which can be observed in Fig. 9 for the Case 2, are most likely not related to the small-scale flow unsteadiness of laminar natural convection flows in closed cavities that is observed above the critical Rayleigh number ~ 3.1×10^5 [32]. These oscillations were observed only in the Case2,

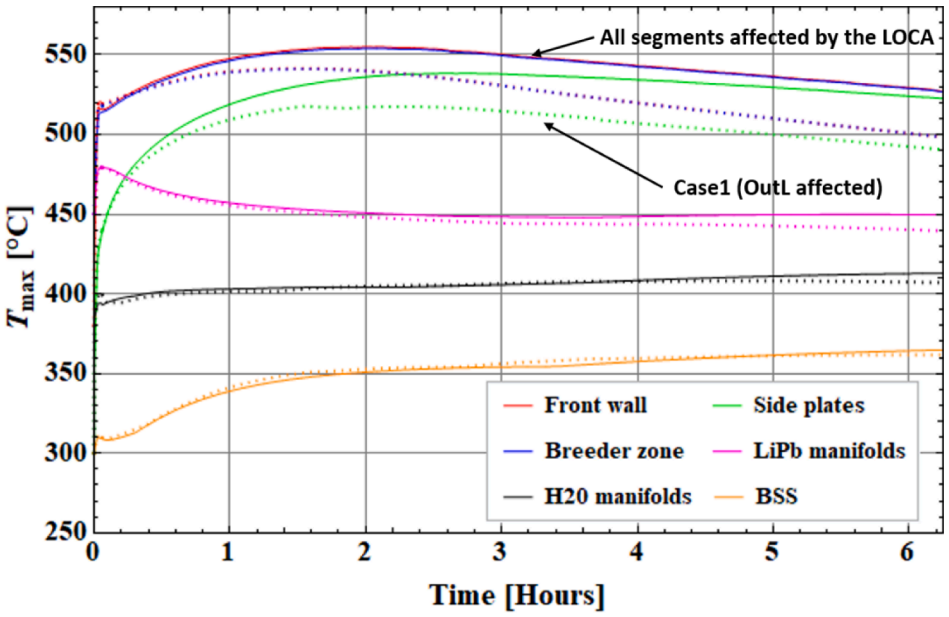

Fig. 10. Time history of peak temperatures in individual blanket layers for outboard lateral (OutL) segment.

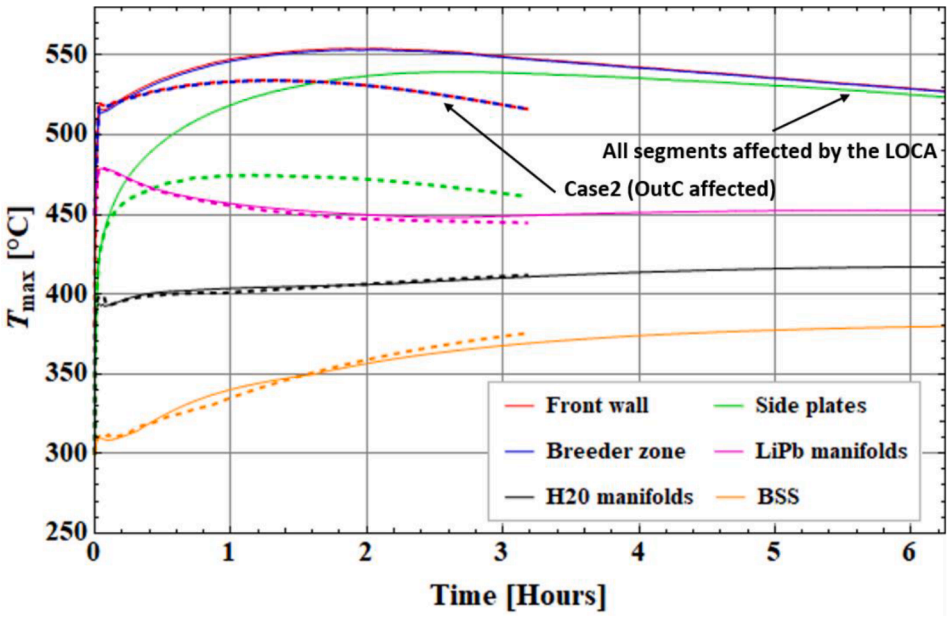

Fig. 11. Time history of peak temperatures in individual blanket layers for the central outboard (OutC) segment.

which has the highest asymmetry in the applied thermal BC for BB (with respect to the left/right side of the domain). Due to the fact that the computational domain includes only 1 VV sector, bounded on both lateral sides by a symmetry boundary condition, it is very likely that the large-scale "pulsating" flow asymmetry the gap (between the back-side InR BB segment and the VV) during the first hour of the simulated transient is numerical artefact, which might be a consequence of the applied boundary conditions that is further enhanced/promoted by the application of flow-freezing strategy. Nevertheless, the cooling trends (for the H2O manifolds and BSS in the Case2) remain similar to other considered cases, indicating that the predicted time-trends are plausible.

4.3. Distribution of thermal loads at external walls of BB segments

The temperature contours at the external surfaces of the BB segments, recorded one hour after the LOCA occurrence, are presented in Fig. 12. Comparison between the simulation Case1 and the conservative case (where all BB segments are affected by the LOCA) shows that in both cases the affected BB segments exhibit a very similar temperature distribution at the external surfaces – the highest temperature occurs at the inner side of the segment (i.e. at the plasma facing side). Quantitatively, the peak temperatures in BB segments are slightly lower when only every second segment is affected by the LOCA (Case1), as the convective cooling on the sidewalls and on the FW of the affected BB segments is more efficient since the surface temperature of adjacent, actively cooled BB segments is somewhat lower than the local temperature of the already heated helium. For example, one hour after the LOCA occurrence the difference in obtained peak BB temperature between the Case1 and the conservative case is about 20 °C (for details see Figs. 9, 10 and 11–), while the maximum surface temperature (occurring

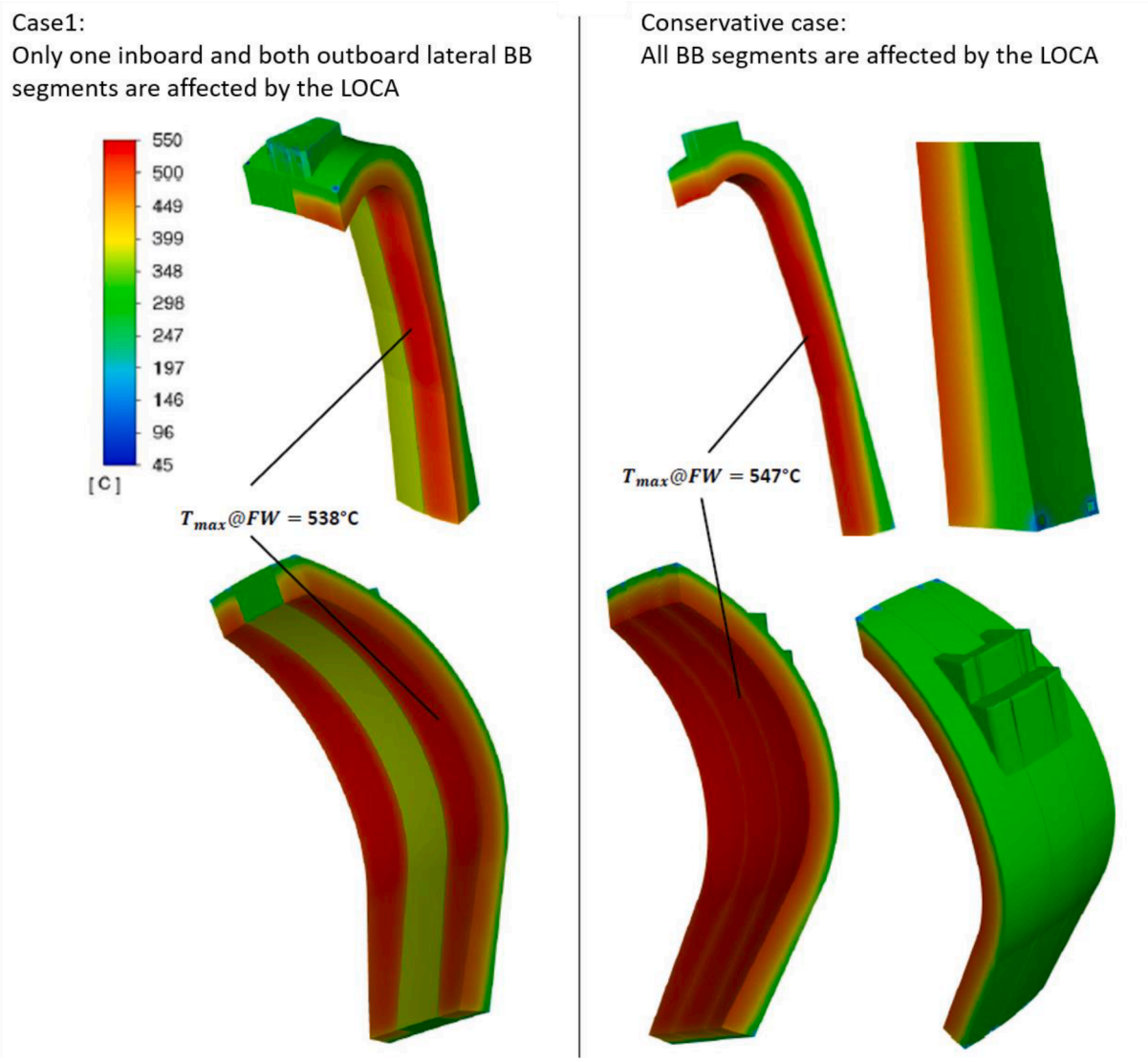

Fig. 12. Temperature contours on external walls of inboard/outboard BB segments.

Table 5
Summary of CFD results (1 hour after LOCA occurrence).

	Heat generation /Total removed heat flow from BB [kW]	BB				
		Total*/ Net radiation power [kW]				Conducted heat flow through supports [kW]
		FW	Side	Back	Chimney	
InL	Actively cooled					
InR**	100.7/113.7	28.9/26.0	27.1/14.7	49.0/12.7	6.3/1.7	2.4
	100.7/130.7	39.3/35.2	32.3/16.7	50.1/13.6	6.6/1.9	2.4
OutL	155.0/184.0	45.0/37.8	42.1/20.2	77.6/20.6	16.0/3.7	3.3
OutR	155.0/181.6	44.9/37.8	39.7/19.2	77.7/20.7	16.0/3.7	3.3
OutC***	165.7/247.8	64.5/51.0	85.8/38.3	70.8/20.0	25.0/5.9	1.7

* Total power comprises the net radiation power and the convective heat transfer.
** Results from simulation Case1 and Case2 are shown in separate lines.
*** Results from simulation Case2 (one inboard and central outboard segments affected).

at the FW) for the Case1 is about 10 °C lower.

Table 5 reports the total heat removed per unit of time (i.e. integral of the surface heat flux) and net radiation power (i.e. integral of the radiation heat flux) that are transferred from affected BB segments through individual external surfaces of the BB segments and chimneys. These values quantify the effectiveness of external BB cooling due to the natural convection and thermal radiation. The contribution of natural convection cooling by filled gas can only be calculated by subtracting the net radiation power from the total power, where the total power refers to the cumulative heat removed per unit of time from the affected BB segments by convection and radiation heat transfer. The first column in Table 5 reports the applied nuclear heats as well as the total heat removed per unit of time, both assessed at one hour after LOCA. At a given instant in time, the removed heat per unit of time in individual

Table 6
Distribution of thermal loads at external walls of BB segments (1 hour after LOCA). Values in brackets correspond to a conservative scenario where all BB segments are affected by LOCA [18].

	Contribution of natural convection cooling at individual external wall* [%]				Fraction of cooling (conv. + rad.) at individual external surface with respect to total removed heat from segment [%]				
	FW	Side	Back	Chimney	FW	Side	Back	Supp.	Chimney
InL**	Actively cooled								
InR	10 (44)	46 (***)	74 (68)	73 (68)	25 (19)	24 (−4)	43 (69)	2 (6)	6 (10)
	10 (44)	48 (***)	73 (68)	71 (68)	30 (19)	25 (−4)	38 (69)	2 (6)	5 (10)
OutL	16 (16)	52 (70)	73 (68)	77 (75)	24 (16)	23 (5)	42 (60)	2 (4)	9 (15)
OutR	16 (23)	52 (72)	73 (68)	77 (73)	25 (17)	22 (6)	43 (59)	2 (4)	9 (14)
OutC	21 (22)	55 (60)	72 (67)	76 (71)	26 (17)	35 (9)	28 (51)	1 (2)	10 (20)

* Contribution of natural convection cooling = (natural conv.) / (natural conv. + radiation).
** actively cooled (one loop of BB PHTS is still operating).
*** The side surfaces of inboard BB segments are being heated due to locally hotter fluid. See [18] for details.

segment is greater than the internal heat generation due to nuclear heating. It is also observed, that the total removed heat per unit of time from the individual BB segments is higher when only every second segment is affected by the LOCA compared to the conservative case where all segments are passive. In the latter case, the total heat removed from the individual BB segments is ~60 kW, ~115 kW and ~120 kW for the inboard, outboard lateral and for the central outboard segments, respectively [18].

The cooling efficiency by natural convection per individual external surface is defined as the fraction between the natural convection cooling and the total removed heat (reported in the first four columns of Table 6). The fraction of total cooling (conv. + rad.) at individual external surface with respect to total removed heat from BB segment is shown in the last five columns of Table 6.

The percentages in the first four columns of Table 6, indicate that the natural convection cooling is the weakest at the plasma facing surfaces (i.e. at FWs), where up to 20% of the removed heat per unit of time occurs due to natural convection. Instead, on surfaces facing the cold VV wall (e.g. through BB back walls, chimneys) the contribution of natural convection cooling is substantially higher (~ 70%). For comparison, the results of conservative case are reported in brackets.

The last five columns of Table 6 report how the achieved cooling is distributed among the individual external surfaces of the segments. It is observed that the highest share of the transferred heat per unit of time occurs through the back wall of the BB segment (up to 45%), while approximately 25% of the cooling is achieved through the front wall. Very similar shares are obtained also through the side surfaces.

For the conservative case [18], it has been noted that the thermalization through the BB back surface is dominating (up to 70%), which is reasonable due to somewhat lower fraction of cooling through the FW and side walls.

5. Conclusions

Temperature response of the Water-Cooled Lithium-Lead (WCLL) breeding blanket [22] during the ex-vessel LOCA in the EU DEMO has been studied by the means of the transient conjugate heat transfer CFD simulation. The postulated guillotine break of a large coolant pipe of the BB Primary Heat Transfer System (PHTS) outside the vacuum vessel (VV) causes an immediate loss of cooling in one (out of two independent) BB cooling loops. As such, only every second BB segment in the toroidal direction is affected by LOCA. For the mitigation of consequences, helium gas is injected into the vacuum chamber, enabling natural convection cooling of affected BB modules. A comparison with a conservative scenario is discussed where it has been assumed that all BB segments (and not only every second) would lose cooling due to the LOCA occurrence [18,19]. Developed three-dimensional CFD simulation model considers thermalization of affected passive BB segments due to established natural circulation of filled gas, heat conduction through physical contacts with actively cooled VV by supports and thermal radiation.

Performed simulations with the ANSYS Fluent code have demonstrated that the decay heat can be effectively removed from passive blanket modules. Peak temperatures in individual BB segments occur within the first two hours from the LOCA occurrence. It has been shown that in cases when every second blanket remains actively cooled, the peak temperature of the affected inboard segments reduces from about 550 °C to about 540 °C. For the central outboard (OutC) segment, the peak temperature decreases from ~555 °C to ~535 °C, and for the outboard lateral (OutL) segment, the peak temperature reduces from ~555 °C to ~540 °C. Natural convection cooling (in respect to thermal radiation) is dominant on the back wall of each BB segment, where about 70% of the heat (heat per unit time) is transferred by moving gas as compared to thermal radiation. This is due the proximity of the cold VV wall. On the other hand, the thermal convection cooling on the front wall (FW) of BB segments is not greater than about 20%. Rather similar distribution of thermal loads is observed in the conservative case where all segments are affected by LOCA [19].

For individual BB segments, about 45% of the cooling is achieved through the back wall, while only 25% of the cooling is provided on the FW and about 25% on the side walls. For the conservative case where LOCA is assumed to affect all segments [19], it has been found that the thermalization through the BB back surface is dominating (up to 70%), which is reasonable due to the slightly lower fraction of cooling through the FW (<20%) and side walls (< 10%).

This study shows that natural convection by injected helium can be considered as a possible mitigation strategy for the decay heat removal from the affected breeding blanket segments during the ex-vessel loss of coolant accident. The simulations show that the peak temperatures in the affected BB segments start to decrease within a few hours after the onset of the accident. However, it should be noted that the performed analysis does not consider any thermal loads on the breeding blanket front walls due to plasma discharges, which could further increase the temperatures in the affected BB segments or eventually cause additional ruptures of the cooling channels in FW of the BB segments that are still actively cooled.

Declaration of generative AI and AI-assisted technologies in the writing process

During the preparation of this work the authors used ChatGPT language model in order to improve language and readability. After using this tool/service, the authors reviewed and edited the content as needed and take full responsibility for the content of the publication.

CRediT authorship contribution statement

Martin Draksler: Formal analysis, Investigation, Methodology, Visualization, Writing – original draft. **Boštjan Končar:** Funding acquisition, Project administration, Writing – review & editing.

Christian Bachmann: Conceptualization, Resources, Writing – review & editing. **Ivo Moscato:** Conceptualization, Writing – review & editing. **Sergio Ciattaglia:** Conceptualization, Writing – review & editing. **Alex Valentine:** Resources, Writing – review & editing.

Declaration of competing interest

The authors declare that they have no known competing financial interests or personal relationships that could have appeared to influence the work reported in this paper.

Data availability

Data will be made available on request.

Acknowledgments

This work has been carried out within the framework of the EUROfusion Consortium, funded by the European Union via the Euratom Research and Training Programme (grant agreement no. 101052200 - EUROfusion). Views and opinions expressed are however those of the author(s) only and do not necessarily reflect those of the European Union or the European Commission. Neither the European Union nor the European Commission can be held responsible for them.

The financial support from the Slovenian Research and Innovation Agency, grant P2-0405, is also gratefully acknowledged.

References

[1] A.J.H. Donne, et al., European Research Roadmap to the Realisation of Fusion Energy, 2018. https://www.eurofusion.org/fileadmin/user_upload/EUROfusion/Documents/2018_Research_roadmap_long_version_01.pdf.
[2] http://www-naweb.iaea.org/napc/physics/meetings/tm45256/talks/Kemp.pdf.
[3] https://www.euro-fusion.org/programme/demo/.
[4] O. Crofts, et al., EU DEMO remote maintenance system development during the pre-concept design phase, Fus. Eng. Des. 179 (2022), https://doi.org/10.1016/j.fusengdes.2022.113121.
[5] M. Coleman, et al., DEMO tritium fuel cycle: performance, parameter explorations, and design space constraints, Fus. Eng. Des. (141) (2019) 79–90, https://doi.org/10.1016/j.fusengdes.2019.01.150. Pages.
[6] G. Federici, et al., An overview of the EU breeding blanket design strategy as an integral part of the DEMO design effort, Fus. Eng. Des. 141 (2019) 30–42, https://doi.org/10.1016/j.fusengdes.2019.01.141.
[7] M. Draksler, et al., Assessment of residual heat removal from activated breeding blanket segment during remote handling in DEMO, FED 173 (2021), https://doi.org/10.1016/j.fusengdes.2021.112891.
[8] IRSN, "Nuclear Fusion Reactor //Safety and Radiation Protection Considerations for Demonstration Reactor that Follow the ITER facility", online publication, https://www.irsn.fr/EN/Research/publications-documentation/Scientific-books/Documents/ITER-VA_web_non_imprimable.pdf.
[9] T. Pinna, et al., Identification of accident sequences for the DEMO plant, Fus. Eng. Des. 124 (2017) 1277–1280, https://doi.org/10.1016/j.fusengdes.2017.02.026. PagesISSN 0920-3796.
[10] B.J. Merrill, et al., A recent version of MELCOR for fusion safety applications, Fus. Eng. Des. 85 (7–9) (2010) 1479–1483, https://doi.org/10.1016/j.fusengdes.2010.04.017. IssuesPagesISSN 0920-3796.
[11] M. D'Onorio, et al., In-box LOCA accident analysis for the European DEMO water-cooled reactor, Fus. Eng. Des. 146 (Part A) (2019) 732–735, https://doi.org/10.1016/j.fusengdes.2019.01.066. ISSN 0920-3796.
[12] M. D'Onorio, et al., Development of a thermal-hydraulic model for the EU-DEMO tokamak building and LOCA simulation, Energ. (Basel) 16 (3) (2023) 1149, https://doi.org/10.3390/en16031149.
[13] X.Z. Jin, BB LOCA analysis for the reference design of the EU DEMO HCPB blanket concept, Fus. Eng. Des. 136 (Part B) (2018) 958–963, https://doi.org/10.1016/j.fusengdes.2018.04.046. PagesISSN 0920-3796.
[14] X.Z. Jin, Preliminary accident analysis of ex-vessel LOCA for the European DEMO HCPB blanket concept, Fus. Eng. Des. 77 (5) (2021) 391–402, https://doi.org/10.1080/15361055.2021.1904769.
[15] A. Zappatore, et al., 3D transient CFD simulation of an in-vessel loss-of-coolant accident in the EU DEMO fusion reactor, Nucl. Fus. 60 (16pp) (2020) 126001, https://doi.org/10.1088/1741-4326/abac6b.
[16] C. Bachmann, Task specification: CFD assessment of natural gas flow in VV during ex-VV LOCA, Priv. Commun. (2021).
[17] M. D'Onorio, et al., Preliminary safety analysis of an in-vessel LOCA for the EU-DEMO WCLL blanket concept, Fus. Eng. Des. 155 (2020), https://doi.org/10.1016/j.fusengdes.2020.111560.
[18] M. Draksler, P. Črne, CFD assessment of natural gas flow in VV during ex-VV LOCA. EFDA_D_2NBVB7, Report for 2021, 2022.
[19] M. Draksler, et al., Natural convection cooling in DEMO vacuum vessel during EX-VV LOCA, in: proceedings: NENE 2022: 31st International Conference Nuclear Energy for New Europe: proceedings: September 12-15, Portorož, Igor Jenčič (ur.), Ljubljana, Nuclear Society of Slovenia, 2022, pp. 1015.1.–11015.8, str.[COBISS.SI-ID 135035651].
[20] M. Draksler, et al., CFD assessment of air flow in VV during in-vessel-component, transport. EFDA_D_2NEUJ7, v. 1.1, Report, 2020.
[21] ANSYS Fluent User's Guide, release 2021.R2.
[22] A. Del Nevo, et al., Recent progress in developing a feasible and integrated conceptual design of the WCLL BB in EUROfusion project, Fus. Eng. Des. 146 (2019) 1805–1809.
[23] A. Valentine, Nuclear heat in FW/BB during ex-vessel LOCA transient. Report, EFDA_D_2NDPJ2 (v1.1), Report, 2021.
[24] C. Bachmann, Task Specifications – CFD Assessment of Air Flow in VV During In-Vessel Maintenance and ex-VV LOCA, PMI-6.1-T016, 2020. Januar.
[25] I. Moscato, et al., Tokamak cooling systems and power conversion system options, Fus. Eng. Des. 178 (2022), https://doi.org/10.1016/j.fusengdes.2022.113093.
[26] M. Draksler, et al., CFD assessment of natural gas flow in the VV and in the upper port transfer cask: associated deliverable DES-ENG.MECHENG.MECHAN-T011-D002, Rev 2.0 (2023) 68, pages. EFDA_D_ 2NL5SQ.
[27] Thermophysical Properties of Materials For Nuclear Engineering: A Tutorial and Collection of Data, IAEA-THPH, IAEA, Vienna, 2008. ISBN 978–92–0–106508–7.
[28] M. Draksler, et al., The effect of mesh refinement on the calculation of cryostat thermal loads in DEMO during the Incident Helium Ingress, in: Proc. 28th Int. Conf. Nuclear Energy for New Europe - NENE 2019, Portorož, Slovenia, 2019, pp. 714.1–714.7. September 9–12.
[29] A. Zappatore, et al., CFD analysis of natural convection cooling of the in-vessel components during a shutdown of the EU DEMO fusion reactor, Fus. Eng. Des. 165 (2021), https://doi.org/10.1016/j.fusengdes.2021.112252.
[30] C.J. Werner, et al., MCNP6.2 Release Notes, Los Alamos National Laboratory, 2018 report LA-UR-18-20808.
[31] T. Eade, et al., Activation and decay heat analysis of the European DEMO blanket concepts, Fus. Eng. Des. 124 (2017) 1241–1245, https://doi.org/10.1016/j.fusengdes.2017.02.100.
[32] J. Oder, I. Tiselj;, Chebyshev collocation benchmark for natural convection flow in differentially heated cavity, AIP Conf. Proc. 1558 (1) (2013) 103–106, https://doi.org/10.1063/1.4825431.